Effects of Spatial Confinement and Selective Distribution of CB Particles on the Crystallization Behavior of Polypropylene

Lan-Peng Li, Jia-Li Wei, Bo Yin, Ming-Bo Yang

College of Polymer Science and Engineering, State Key Laboratory of Polymer Materials Engineering, Sichuan University, Chengdu, Sichuan 610065, People's Republic of China

Received 11 January 2011; accepted 3 June 2011
DOI 10.1002/app.35032
Published online 22 September 2011 in Wiley Online Library (wileyonlinelibrary.com).

ABSTRACT: The effects of selective distribution of carbon black (CB) particles and spatial confinement on the crystallization behavior of isotactic polypropylene (iPP)/Polystyrene (PS)/CB composite were studied. The crystallization behaviors and the morphologies of the composite were studied by differential scanning calorimetry (DSC), polarized light microscope (PLM), and scanning electron microscopy (SEM). The results indicated the typical cocontinuous structure appeared in PP/PS/CB (55/45/1) composite, and CB particles are distributed in PS phase, which follows the theory of interfacial tension. Compared with PP/CB composite, the nucleation effect of CB particles on the crystallization process of PP in PP/PS/CB was greatly weakened by selective distribution. Moreover, the morphologies of cocontinuous structure, which means that the crystallization process of PP had to take place in the micron-scale spatial confinement formed by continuous PS phase, greatly influenced the crystallization behavior of PP in PP/PS/CB composite. The spherulite radial growth rate of PP in spatial confinement was lower than that of neat PP during isothermal crystallization processes, and the results of the total crystallization activation energy (ΔE) and the nucleation parameter (K_t) implied that in comparison to neat PP, the activation energy of PP chain segments arranged into crystal was higher in composite with cocontinuous structure. © 2011 Wiley Periodicals, Inc. J Appl Polym Sci 123: 3652–3661, 2012

Key words: crystallization; morphology; poly(propylene); selective distribution; spatial confinement

INTRODUCTION

To obtain better properties of polymer materials, polymer blends or polymer/filler composites have been widely applied as a versatile method in the industry because of their ability to tailor materials for specific applications, at a relatively low cost when compared with the development of a new polymer.[1–6] However, it is well known that the properties of polymer composites greatly depend on the micromorphology and crystallization behavior. Therefore, the studies concerning the crystallization behavior of polymer composites have attracted great interest from researcher in recent years.[7–9]

The crystallization behavior of polymer can be obviously influenced by the presence of another polymer component or fillers. Recently, studies on the crystalline/amorphous polymer blends have been appearing. These systems include polypropylene (PP)/ethylene–propylene–diene rubber (EPDM) blends,[10,11] PP/MPP blends,[12] PE/PC blends,[13] etc. On the other hand, the crystallization behaviors of polymer/filler composites have been carried out extensively too. Nowadays, various inorganic fillers (especially in the nanoscale) are added into polymer matrix for the purposes of enhancing the special performances of polymer materials, such as increase of modulus and strength, electrical conductivity, improved barrier properties, increase in solvent and heat resistance, and enhancement of good optical transparency. Moreover, the fillers usually include mica,[14] montmorillonite,[15] whiskers,[16] fiber,[17] carbon fiber,[18] carbon black,[19] carbon nanotubes,[20] calcium carbonate ($CaCO_3$),[6] etc. In general, the addition of nanofillers can largely change the crystallization behavior of crystalline polymer (increasing the crystallization rate and the crystallization temperature, etc). However, for polymer blends/inorganic filler composites, the selective distribution of inorganic filler is a key factor which greatly influences the performance of composites. Up to now, several theories have been established to study the selective distribution of fillers in polymer blends. Theory of interfacial tension proposed that the fillers prefer to migrate to the phase whose interfacial tension with the filler was lower than the other phase to reduce

Correspondence to: B. Yin (yinbo@scu.edu.cn).
Contract grant sponsor: National Natural Science Foundation Commission of China; contract grant numbers: 20874066, 50903050.

the whole free energy of composite.[21] Most of the studies have confirmed the accuracy of interfacial tension model.[22,23] Moreover, some other scholars[24] also reported that when the viscosities of two polymers are incomparable, fillers will come into the phase with lower viscosity to minimize the dissipative energy of composite.

It is well known that morphology is a key determinant of the final properties of polymer blends, so it is interesting that how to change the crystallization process and crystal morphology. Up to now, many works have been done to control the crystallization behavior of polymer by changing the crystallization temperature, pressure, cooling rate, etc. However, to our knowledge, the study of crystallization process of polymer in the spatial confinement has received very little attention. Thus, in this work, PP/PS/CB composite with cocontinuous structure were prepared by melt mixing. Then the crystallization behavior of PP in the spatial confinement was studied. Moreover, the effect of selective distribution of CB particles on the crystallization behavior of PP in PP/PS/CB composite was also studied here. The final purpose of the work is to understand the influencing factors of polymer crystallization, so that the properties of polymer blends/composites can be improved by controlling the process of polymer crystallization.

EXPERIMENTAL PART

Materials

Isotactic polypropylene (iPP, T30S) was purchased from Lanzhou Petrochemical Company, China; it has a melt flow rate (MFR) of 2.6 g/10 min (ASTM D1238.79) and mass density of 0.91 g/cm^3 (ASTM D1505-68). Polystyrene (PS, 630A) was supplied by (Dow Chemical Company, USA); it has a melt flow rate (MFR) of 3 g/10 min (ASTM D1238.79) and mass density of 1.04 g/cm^3 (ASTM D1505-68). Carbon black CB (CB, BP2000) was purchased by Cabot (American); it has an average diameter of 12 nm.

Sample preparation

Before blending, all materials were dried at 80°C for about 8 h, to minimize the effects of moisture. All blends/composites were prepared by melt mixing on a CTE35 corotating twin screw extruder (KEYA Company, Nanjing, China) at 200°C and the screw speed maintained at 100 rpm. Then, the extrudate strands were pelletized and dried at 80°C for 8 h before characterizations. All blend ratios described are related to weight ratios.

Scanning electron microscopy (SEM)

The samples were fractured in liquid nitrogen and the fractured surfaces were observed with a FEI INSPECT F scanning electron microscope (New York). All samples were sputter coated with gold and observed with an acceleration voltage of 20 kV.

Contact angle measurements

Contact angles were measured in a sessile drop mold with KRÜSS DSA100 (German). PP and PS samples were compression molded between clean silicon wafers at 200°C for 3 min and then cooled to 25°C under pressure for 1 min. CB powders were compression molded at room temperature under a certain pressure. Contact angles were measured on 3 μL of wetting solvent (water and diiodomethane) at 20°C.

Polarized light microscope (PLM)

A polarized light optical microscope equipped with a hot plate was used to study the crystal morphology and the isothermal spherulite growth rate of neat PP and PP/PS/CB composite. The samples sandwiched between two microscope cover slips were first pressed into thin film samples at 200°C, and then maintained at 200°C for 5 min. The temperature of the hot plate was then cooled to the crystallization temperature (T_c) at a rate of 100°C/min. The crystallization process was recorded by taking photographs at constant time intervals. The radial growth rate of spherulites was determined by measuring the radii of the growing spherulites as a function of time.

Differential scanning calorimetry (DSC)

The crystallization behavior of PP in the blends prepared was analyzed using about 5 mg samples by a TA Q-20 Differential Scanning Calorimeter (Boston) under a nitrogen atmosphere. Nonisothermal crystallization were studied through following sequences: After eliminating the thermal history of the samples by heating up to 200°C at a heating rate of 50°C/min and maintaining for 5 min, the samples were cooled down to 50°C at a cooling rate of 10°C/min, and then heated to 200°C at a heating rate of 10°C/min. Both cooling and heating curves were recorded for analysis.

In isothermal crystallization studies, the removal of the thermal history of the samples was accomplished through the exactly same procedures as in nonisothermal crystallization studies. Sequentially, the samples were rapidly (80°C/min) cooled to the crystallization temperature (T_c) and maintained at

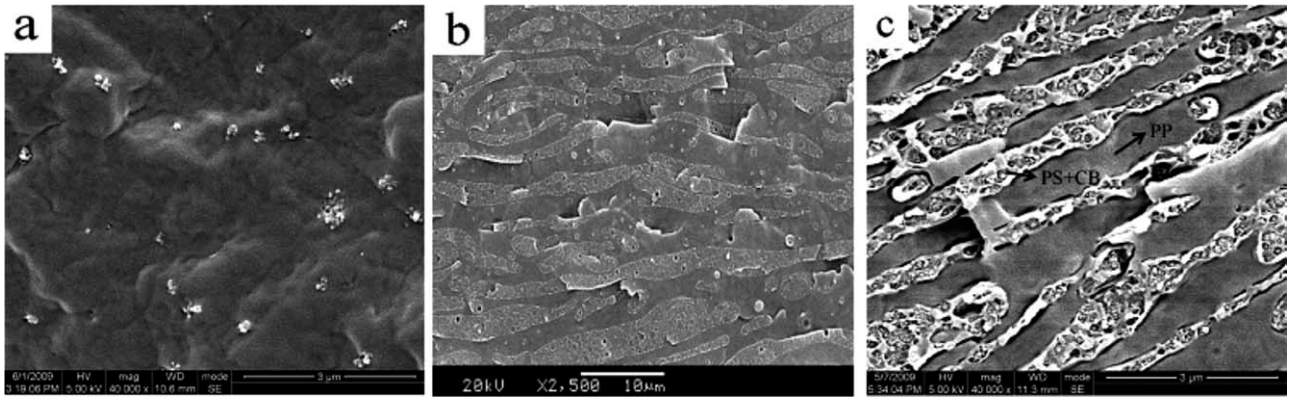

Figure 1 SEM photos of fracture surface of different samples. (a) PP/CB 100/1; (b) PP/PS 55/45; and (c) PP/PS/CB 55/45/1.

that temperature for sufficiently long time to ensure the complete crystallization of PP matrix. Four T_c values of 122, 124, 126, and 128°C were chosen. After the isothermal crystallization was finished, the samples were heated to 200°C at a rate of 10°C/min.

Wide-angle X-ray diffraction (WAXD)

WAXD measurement was carried out with a DX-1000 X-ray diffractometer at room temperature. Before testing, the samples were heated up to 200°C at a rate of 50°C/min under a nitrogen atmosphere and held there at 50°C for 5 min to eliminate the thermal history. Afterward, the samples were rapidly (80°C/min) cooled to the crystallization temperature (T_c) and maintained at that temperature for sufficiently long time to ensure the complete crystallization of PP matrix. The Cu K-alpha (wave length = 0.154056 nm) irradiation source was operated at 50 kV and 30 mA. The patterns were recorded by monitoring the diffractions from 5° to 50°, and the scanning speed was 3°C/min.

RESULTS AND DISCUSSIONS

SEM observation

It is well known that the dispersion of filler in polymer matrix is critical to the properties of polymer composites. The morphology of PP/CB (100/1) is shown in Figure 1(a), the agglomerates of CB particles can be easily observed because of the thermodynamics factors.[25] While for the PP/PS blend, the typical cocontinuous structure appeared in the PP/PS (55/45) blend according to Figure 1(b). When CB particles were added to PP/PS blend, the cocontinuous structure still existed. Furthermore, it is interesting to find the selective distribution of CB particles in PP/PS matrix. CB particles were preferentially distributed in the PS phase [seen in Fig. 1(c)]. Similar phenomenon was reported by Uttandaraman Sundararaj and coworkers.[26]

To understand the mechanism of selective distribution of CB particles in the PP/PS matrix, some thermodynamic and kinetic factors should be taken into account. Interfacial tension is considered first. Specifically, the contact angles of the raw materials with water and diiodomethane are listed in Table I. As a result, the surface tension, dispersion, and polar components of materials are calculated by eqs. (1) and (2),[27,28] as listed in Table I.

$$(1+\cos\theta_{H_2O})\gamma_{H_2O} = 4\left(\frac{\gamma^d{}_{H_2O}\gamma^d}{\gamma^d{}_{H_2O}+\gamma^d}+\frac{\gamma^p{}_{H_2O}\gamma^p}{\gamma^p{}_{H_2O}+\gamma^p}\right) \quad (1)$$

$$(1+\cos\theta_{CH_2I_2})\gamma_{CH_2I_2} = 4\left(\frac{\gamma^d{}_{CH_2I_2}\gamma^d}{\gamma^d{}_{CH_2I_2}+\gamma^d}+\frac{\gamma^p{}_{CH_2I_2}\gamma^p}{\gamma^p{}_{CH_2I_2}+\gamma^p}\right) \quad (2)$$

where γ is the surface tension, γ^d is the dispersion component, γ^p is the polar component, and θ is the contact angle with water or diiodomethane.

Furthermore, the interfacial tension was calculated by Wu's equation [Eq. (3)],[27] where γ_{12} is the interfacial tension between materials 1 and 2, γ_1 and γ_2 are the surface tensions of the two contacting components in the composites.

TABLE I
Summary of Contact Angle and Surface Tension of Different Materials

	Contact angle (°)		Surface tension (mN/m)		
Sample	Water	Diiodomethane	Total (γ)	Dispersion component (γ^d)	Polar component (γ^p)
PP	103.2	51.1	38.5	38.4	0.1
PS	92.4	59.3	31.38	25	6.38
CB	46.2	13.8	61.6	35.6	26

TABLE II
The Values of the Interfacial Tension of Different Materials

Possible pairs	Interfacial tension (m*N*/m)
PP-CB	25.8
CB-PS	13.7

$$\gamma_{12} = \gamma_1 + \gamma_2 - 4\left(\frac{\gamma^d{}_1\gamma^d{}_2}{\gamma^d{}_1 + \gamma^d{}_2} + \frac{\gamma^p{}_1\gamma^p{}_2}{\gamma^p{}_1 + \gamma^p{}_2}\right) \quad (3)$$

Usually, the most stable phase morphology of a multicomponent polymer system must be corresponding to the lowest free energy, and the free energy of the system decreases as the lower interfacial tension. Correspondingly, according to the results in Table II, CB particles prefer to stay in PS phase because of the lowest γ_{12} (13.7 m*N*/m). This can explain the phase morphology of PP/PS/CB in Figure 1.

PLM observation

The crystal morphologies and the spherulite radial growth rate of polymer materials can be observed by PLM. Here, the addition of CB which was distributed in PS phase can increase the contrast between PP phase and PS phase. Figure 2 presents the crystal growth of neat PP and PP phase in PP/PS/CB composite at the T_c of 122°C at the time of 80, 100, and 140 s in sequence. In PP/PS/CB composite, many nucleation and crystallization processes began at the interface between PP phase and PS/CB phase, which

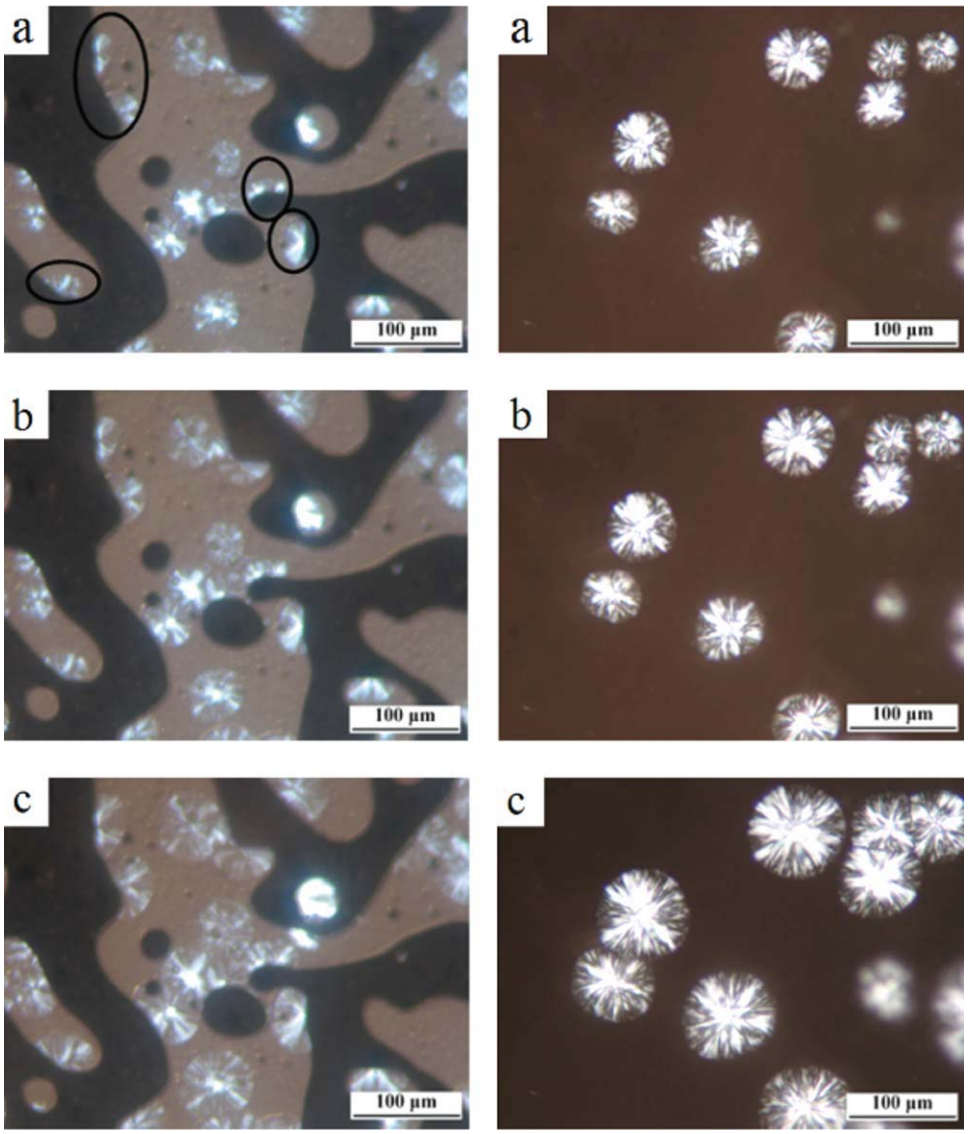

Figure 2 The crystal morphologies of neat PP (right) and PP/PS/CB (55/45/1) (left) crystallized at 122°C. Crystallization time: (a) 80 s, (b) 100 s, and (c) 140 s. [Color figure can be viewed in the online issue, which is available at wileyonlinelibrary.com.]

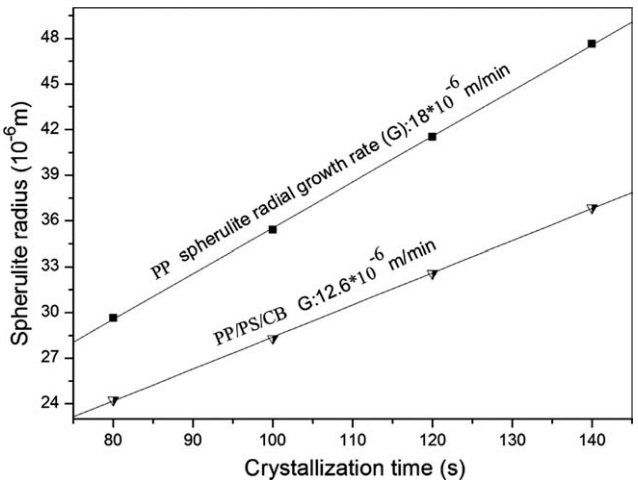

Figure 3 Plots of the spherulite radius versus crystallization time for neat PP and PP/PS/CB (55/45/1).

can be ascribed to the nucleation effect of PS/CB on the crystallization of PP. At the same time, the spherulite radius as a function of crystallization time at 122°C is given in Figure 3. For both samples, a linearly increasing of the spherulite size with time exists before the impingement of the spherulites. The spherulite radial growth rate (G) can be obtained by calculating the slopes of regression lines in Figure 3. The G value of neat PP is bigger than that of PP/PS/CB composite, implying that movement ability of PP chain segments were decreased when they were arranged into crystal.

DSC results

Nonisothermal crystallization behavior of neat PP, PP/CB, PP/PS, and PP/PS/CB

To further understand the difference of the spherulite radial growth rate between neat PP and PP in PP/PS/CB composite, DSC experiments including nonisothermal crystallization and isothermal crystallization were measured.

Figure 4 shows the DSC cooling and heating curves of the PP, PP/CB, PP/PS, and PP/PS/CB. The results of the nonisothermal crystallization according to Figure 4 are summarized in Table III. Here, the peak temperature and onset temperature of crystallization and melting process are designated as $T_{C\text{-}Max}$, $T_{C\text{-}onset}$, $T_{H\text{-}Max}$, and $T_{H\text{-}onset}$, respectively. Obviously, when CB particles and PS resin were added to PP matrix, the crystallization and melting behavior of PP phase in the blend/composite changes remarkably. Compared with neat PP, higher $T_{C\text{-}onset}$ and $T_{C\text{-}Max}$ happened to the PP/CB, PP/PS, and PP/PS/CB. Moreover, the highest $T_{C\text{-}onset}$ (127.7°C) and $T_{C\text{-}Max}$ (124.3°C) value are corresponding to the PP/CB. This result indicates that both CB particles and PS resin can act as the nucleating agent for PP crystallization with CB particles having better nucleating efficiency. It is well known that more perfect crystal structure usually leads to higher melting temperature.[29] According to Table III, $T_{H\text{-}onset}$ and $T_{H\text{-}Max}$ of PP phase in the PP/CB composites shift to 158.4 and 163.2°C, respectively, from 155.3 and 160.4 of neat PP. This can be attributed to better nucleating efficiency of CB particles which could perfect crystal structures in PP. While it is found that almost equal $T_{C\text{-}onset}$, $T_{H\text{-}onset}$, and $T_{H\text{-}Max}$ value can be seen between PP/PS/CB and PP/PS composites. This indicates the effect of the selective distribution of CB particles on the crystallization behavior of PP in PP/PS/CB composite. It seems that when CB particles were preferentially distributed in the PS phase, the crystallization behaviors of PP in PP/PS/CB composite were not influenced by CB particles.

Isothermal crystallization of PP, PP/CB, PP/PS, and PP/PS/CB

Based on the change of heat flow with time, depicted in Figure 5, the development of the relative crystallinity of pure PP with time at different T_c

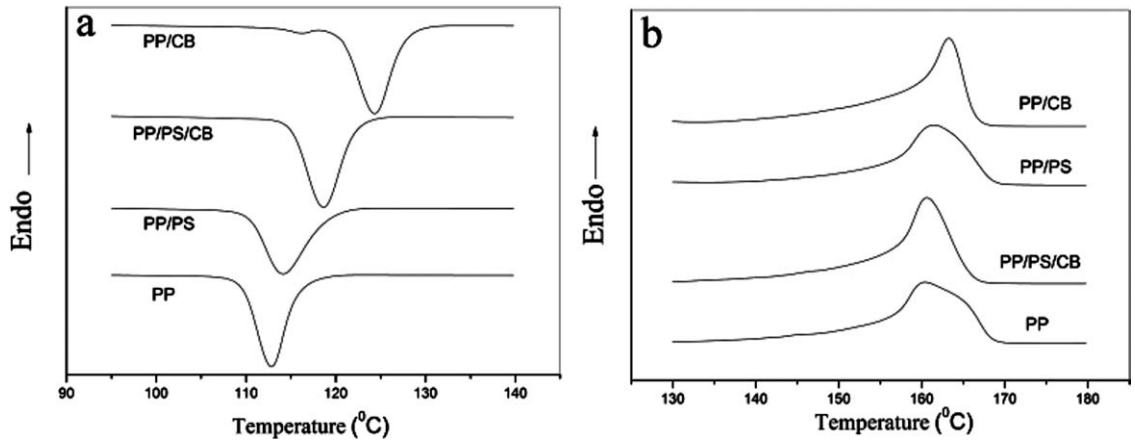

Figure 4 Nonisothermal crystallization and melting behaviors of neat PP, PP/CB (100/1), PP/PS (55/45), and PP/PS/CB (55/45/1). (a) Crystallization exotherms (cooling rate: 10°C/min); (b) melting process (heating rate: 10°C/min).

TABLE III
Various Parameters of Neat PP, PP/CB (100/1), PP/PS (55/45), and PP/PS/CB (55/45/1) Determined from the Nonisothermal Crystallization and Melting Processes

	Cooling scan		Heating scan	
Samples	$T_{C\text{-onset}}$ (°C)	$T_{C\text{-Max}}$ (°C)	$T_{H\text{-onset}}$ (°C)	$T_{H\text{-Max}}$ (°C)
PP	115.7	112.8	155.3	160.4
PP/CB	127.7	124.3	158.4	163.2
PP/PS	123.0	114.6	155.6	161.4
PP/PS/CB	122.1	118	155.9	160.5

were recorded according to Eq. (4), as shown in Figure 6(a). Accordingly, the plots of relative crystallinity versus time of the PP/PS (55/45), PP/CB (100/1), and PP/PS/CB (55/45/1) composites with at different T_c are recorded and shown in Figure 6(b–d), respectively.

$$X(t) = Q_t/Q_\infty = \int_0^t (dH/dt)dt / \int_0^\infty (dH/dt)dt \quad (4)$$

where Q_t and Q_∞ are the heat generated at time t and infinite time t_∞, respectively, and dH/dt is the rate of heat evolution.

Figure 6 shows the development of the relative crystallinity of neat PP and PP in PP/CB, PP/PS, and PP/PS/CB with time at different crystallization temperature (T_c). The half crystallization time ($t_{1/2}$) defined as the time required to 50% crystallinity is a characteristic parameter describing the overall crystallization rate, and it can be easily read from Figure 6 and was given as a function of T_c in Figure 7. It can be seen that the overall crystallization rates of all materials decrease as T_c increases from 395 to 401 K. The crystallization rates of all composite/blend are higher than that of neat PP, whereas the highest crystallization rate (lowest $t_{1/2}$) occurs in PP/CB composite at any T_c. The results further suggest the role of CB particles and PS resin as nucleating agents for PP crystallization and better nucleating efficiency of CB particles, in good agreement with the nonisothermal crystallization results. However, it is found that $t_{1/2}$ of PP in PP/PS is higher than that of PP in PP/PS/CB. This suggests that the nucleating efficiency of PS/CB is higher than that of PS. It is inferred that a small quantity of CB particles which are distributed on the interface between PP and PS can enhance the crystallization nucleation rate. The CB distributed on the interface was effectless with enhancing the crystallization temperature in the nonisothermal crystallization process (seen in Table III), which may be caused by limited quantity of CB particles and overquick cooling rate (10°C/min).

The Avrami equation[30,31] is also applied to analyze the isothermal crystallization of PP and its composites, as given in Eq. (5):

$$1 - X(t) = \exp(-Zt^n) \quad (5)$$

$$1g[-\ln(1 - X(t)] = \lg Z + n \lg t \quad (6)$$

where Z is the Avrami rate constant containing the nucleation and the growth parameters, n is the Avarami exponent whose value depends on the mechanism of nucleation and on the form of crystal growth, t is the time of crystallization, $X(t)$ is related to the relative crystallinity at time t, which can be obtained from the ratio of the area of the exotherm up to time t divided by the total exotherm [given in Eq. (4)]. From a graphic representation of $\log[-\ln(1 - X(t))]$ versus $\log t$, the Avrami exponent n (slope of the straight line) and the crystallization kinetic constant Z (intersection with the y-axis) can be obtained. Plots of $\log[-\ln(1 - X(t))]$ versus $\log t$ are shown in Figure 8. Each curve shows the only linear portion. The results from Figure 8 are listed in Table IV. The Avrami exponent n depends on the nucleation process and the geometry of the growing crystals.[31] As shown in Table IV, the values of n of the PP/CB composites are higher than that in pure PP. The increase of n value is usually attributed to the change from instantaneous to sporadic nucleation.[32] Moreover, the crystallization rate parameter Z is very dependent on the crystallization temperature T_c. As T_c increased, the K value is significantly decreased. At a given crystallization temperature, the addition of CB particles or PS phase can increase K value obviously, which also verifies the nucleating effect of CB particles and PS phase.

The crystallization thermodynamics and kinetics of polymer materials have been described by the crystallization nucleation theory of Hoffman and Lauritzen.[33] The L-H model can be written as follows:

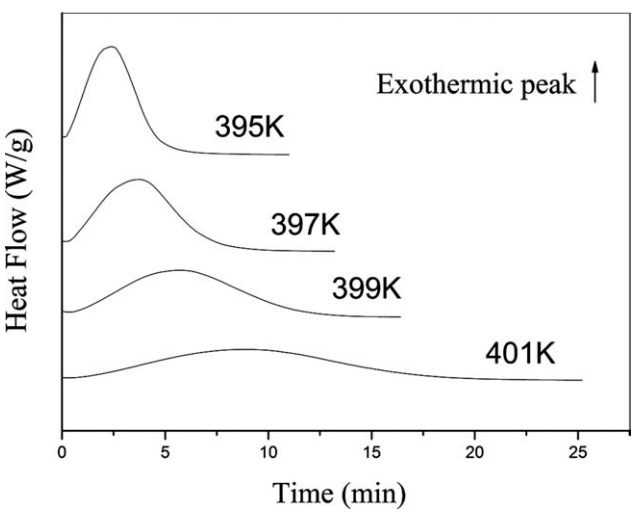

Figure 5 Heat flow as a function of time during isothermal crystallization at the different crystallization temperatures for neat PP.

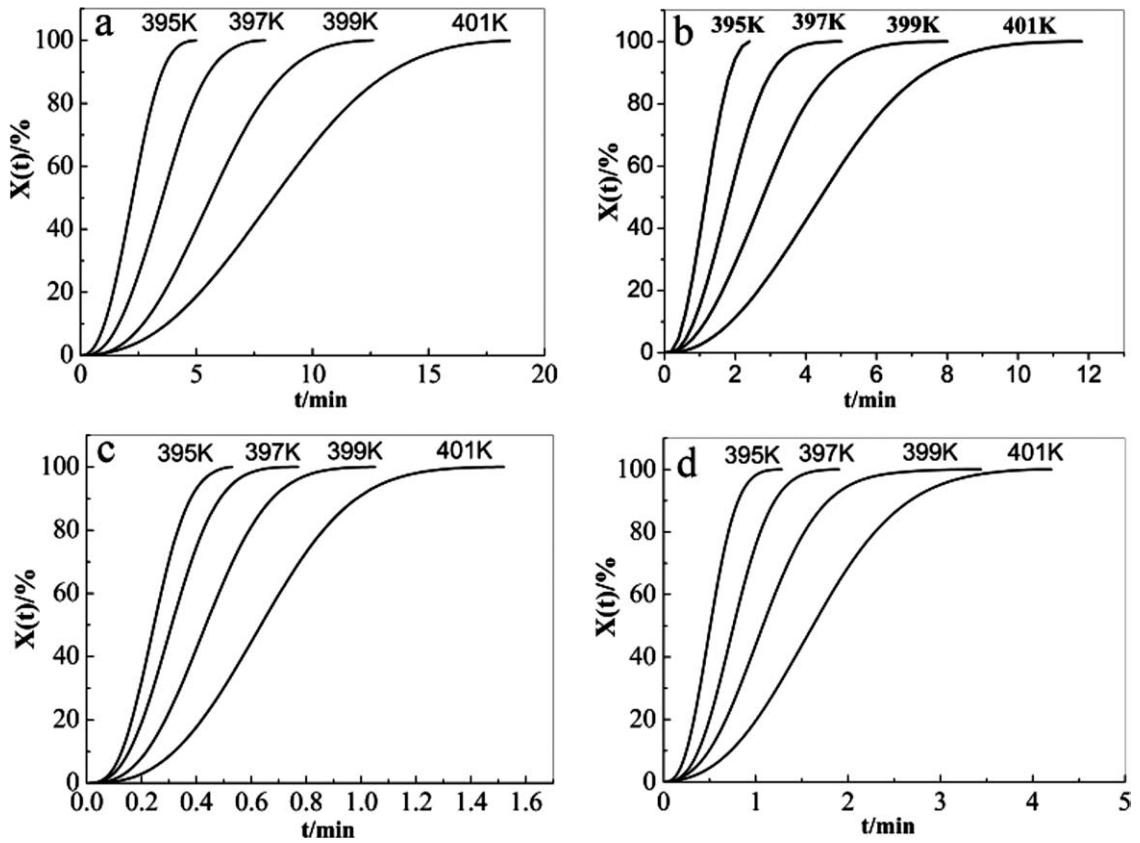

Figure 6 Development of the relative crystallinity with time during isothermal crystallization at different T_c for (a) PP, (b) PP/PS (55/45), (c) PP/CB (100/1), and (d) PP/PS/CB (55/45/1).

$$G = G_0 \exp\left[-\frac{U^*}{R(T_C - T_\infty)}\right] \exp\left[-\frac{K_g}{T_C \Delta T}\right] \quad (7)$$

$$\ln G + \frac{U^*}{R(T_C - T_\infty)} = \ln(G_0) - \frac{K_g}{T_C \Delta T} \quad (8)$$

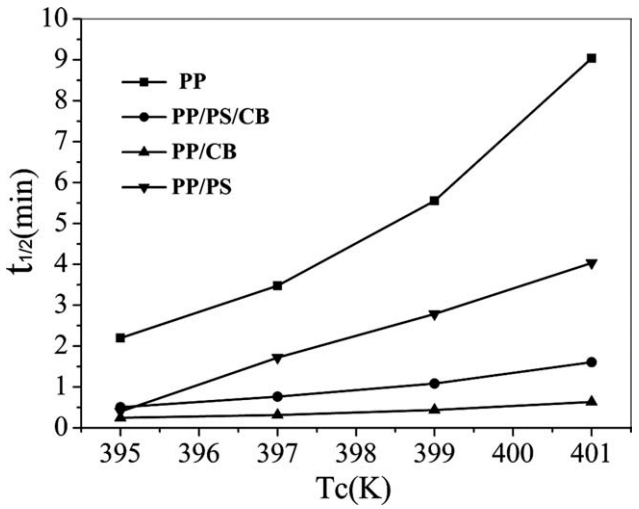

Figure 7 Plots of $t_{1/2}$ versus T_c for the isothermal crystallization of neat PP, PP/CB (100/1), PP/PS (55/45), and PP/PS/CB (55/45/1).

where, G is growth rate; G_0 is a preexponential factor; h-Planck constant; U^*—activation energy for the transport process at the liquid–solid interface; K_g—nucleation parameter; $T_\infty = T_g - C$ ($C \approx 30K$); T_c—crystallization temperature; $\Delta T = T_m^0 - T_c$; T_m^0—equilibrium melting temperature. Moreover, U^* is usually given by a universal value of 1500 cal/mol, and the typical values of the glass transition temperature (T_g) 261.2 K and the equilibrium melting temperature (T_m^0) 458.2 K for isotactic PP were used in this work.[34] The extended Lauritzen–Hoffmann equation[35] can be written also for the half time of crystallization.

$$\frac{1}{t_{1/2}} = \left(\frac{1}{t_{1/2}}\right)_0 \exp\left[-\frac{U^*}{R(T_C - T_\infty)}\right] \exp\left[-\frac{K_t}{T_C \Delta T}\right] \quad (9)$$

$$-\ln t_{1/2} + \frac{U^*}{R(T_C - T_\infty)} = \ln\left(\frac{1}{t_{1/2}}\right)_0 - \frac{K_t}{T_C \Delta T} \quad (10)$$

where $(1/t_{1/2})_0$ a preexponential factor and K_t is nucleation parameter which can be determined by the fitting of Eq. (10) to experimental points.

Based on the theory of extended L-H model, the nucleation parameter (K_t) can be obtained by simulating the slope of the plots of ($\ln t_{1/2} + U^*/R$ ($T_c - T$)) verse $1/(T_C \Delta T)$ [according to Eq. (10)]. The

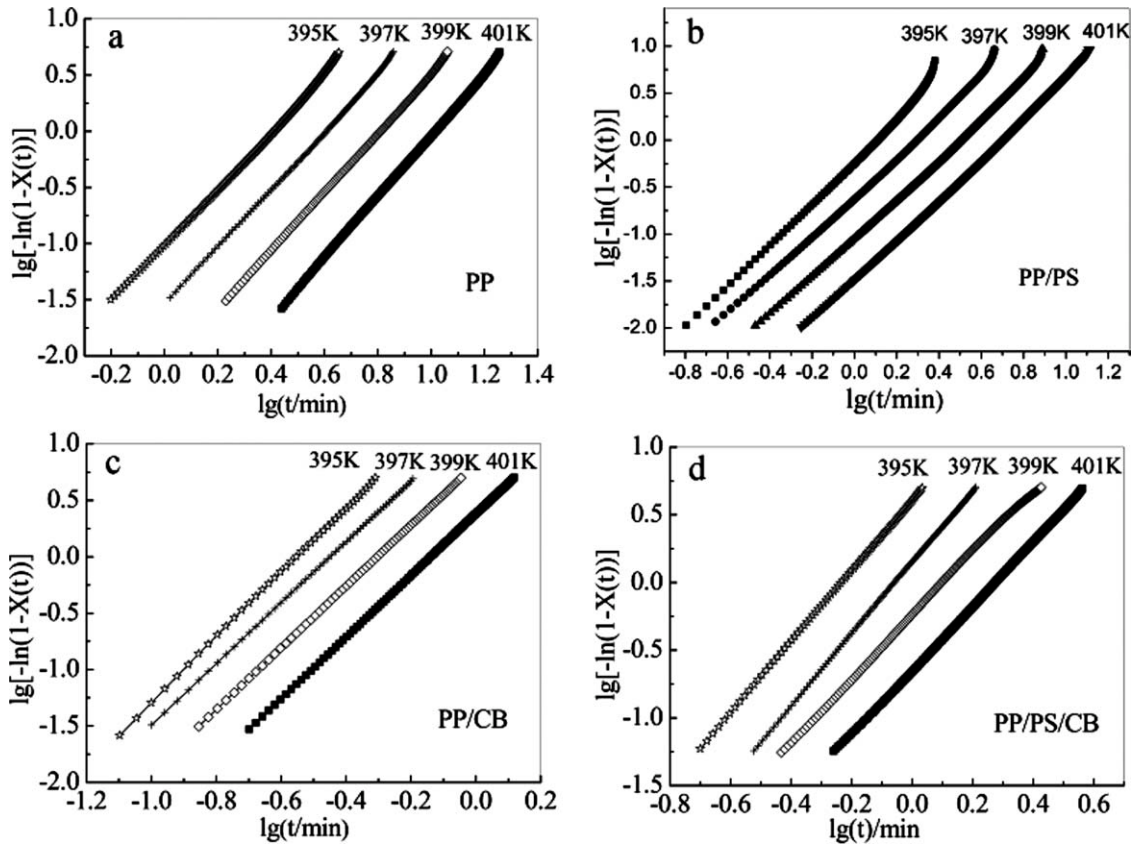

Figure 8 Avrami plots for isothermal crystallization of different samples. (a) neat PP, (b) PP/PS 55/45, (c) PP/CB 100/1, and (d) PP/PS/CB 55/45/1.

higher K_t associates with higher nucleation activation energy. Figure 9 shows the plots of Eq. (10) for PP, PP/CB, PP/CB, and PP/PS/CB. The relationship of K_t (neat PP)>K_t (PP/PS)>K_t (PP/PS/CB)>K_t (PP/CB) is clearly presented. Because of the relation between K_t and nucleation activation energy, it is more difficult to nucleate for neat PP compared with PP in PP/CB, PP/PS, and PP/PS/CB.

To understand the crystallization process of neat PP, PP/CB, PP/PS, and PP/PS/CB well, not only nucleation stage but also crystal growth process should be investigate. The total crystallization activation energy (ΔE) which includes nucleation and

TABLE IV
Results of the Avrami Analysis for Isothermal Crystallization of iPP, PP/PS, PP/CB, and PP/PS/CB [Determined from Eq. (6)]

Samples	T_c (K)	n	lnZ
iPP	395	2.55	−2.37
	397	2.57	−3.57
	399	2.62	−4.86
	401	2.72	−6.36
PP/PS (55/45)	395	2.656	−0.76
	397	2.628	−2.02
	399	2.248	−2.62
	401	2.321	−3.76
PP/CB (100/1)	395	2.86	3.64
	397	2.70	2.76
	399	2.72	1.89
	401	2.73	0.87
PP/PS/CB (55/45/1)	395	2.61	1.40
	397	2.64	0.35
	399	2.33	−0.55
	401	2.38	−1.50

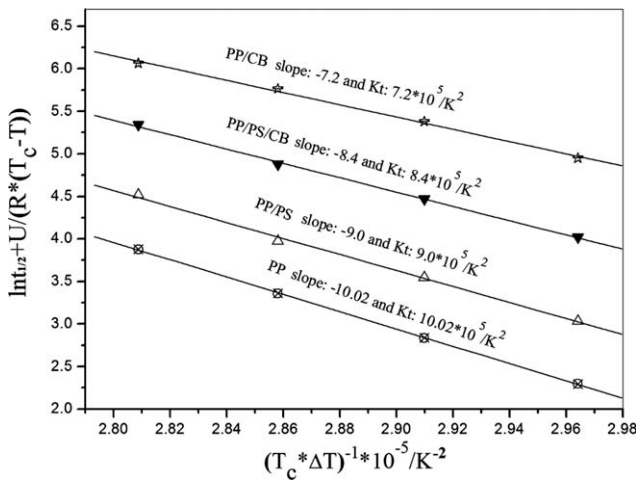

Figure 9 Plots of Eq. (10) for neat PP, PP/CB (100/1), PP/PS (55/45), and PP/PS/CB (55/45/1).

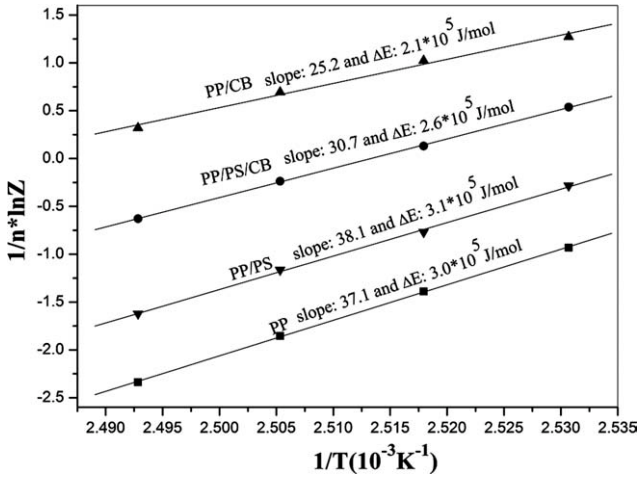

Figure 10 Plots of $(1/n)(\ln Zt)$ versus $1/T_c$ for neat PP, PP/CB (100/1), PP/PS (55/45), and PP/PS/CB (55/45/1).

crystal growth process can be approximately described by the following Arrhenius equation[36]:

$$Z^{1/n} = Z_0 \exp\left(\frac{-\Delta E}{RT_C}\right) \tag{11}$$

$$\left(\frac{1}{n}\right) \ln Z = \ln Z_0 - \frac{\Delta E}{RT_C} \tag{12}$$

where, Z—the crystallization rate parameter; Z_0—the temperature-independent preexponential factor; R—the gas constant; ΔE—the total crystallization activation energy (the slope coefficient of plots of $(1/n)\ln Z$ versus $(1/T_c)$, which is shown in Figure 10.

Because of the nucleating efficiency of PS phase, the K_t value of PP in PP/PS is less than neat PP (seen in Fig. 9). However, it is found that the total crystallization activation energy (ΔE) of PP in PP/PS blend is greater than that of neat PP (seen in Fig. 10). This implies that compared with neat PP, higher activation energy was needed in crystal growth process of PP in PP/PS blend, which means higher the activation energy of PP chain segments arranged into crystal appears in PP/PS blend. Moreover, because CB particles were distributed in PS phase, the crystal growth of PP in PP/PS/CB was not influenced by CB particles. It can be inferred that the crystal growth activation energy of PP in PP/PS/CB is equal to that of PP in PP/PS which is higher than the crystal growth activation energy of neat PP. This result provides a good explanation for lower spherulite radial growth rate of PP phase in PP/PS/CB than that of neat PP (seen in Fig. 3).

WAXD results

Figure 11 shows the WAXD profiles of the composite samples isothermally crystallized at 122°C. It is observed that the peaks at diffraction angles 2θ of 14°, 16.8°, and 18.5° are attributed to α (110), α (040), and α (130) planes in Figure 11, respectively. However, the peak at diffraction angle 2θ of 16° attributed to β (300) is absent for the WAXD profiles of all samples. This indicates that only α-crystal formed in all samples, and the crystal structure of iPP is not influenced by CB particles and PS phase.

Effect of spatial confinement on the crystallization of PP

Figure 1 shows the SEM photos of the morphology of PP/PS and PP/PS/CB. As seen in Figure1(b,c), the addition of CB did not change the morphology of PP/PS blend. So, the typical cocontinuous structure was observed in the PP/PS and PP/PS/CB. The cocontinuous morphology, in other words, is the structure of confining morphologies each other in the microscale. Here, in the PP/PS and PP/PS/CB, PP phase became continuous fiber-like structures [see Fig. 1(c)] because of the confinement effect of PS phase. Moreover, it can be seen in Figure 2 that the crystallization of PP took place on the interface between PP and PS because of the heterogeneous nucleation effect of PS resin or CB distributed on the interface. It is well known that the shrinkage behavior can be caused by crystallization process of polymer, so a drawing force would be caused by the shrinkage behavior. Because in the confined space of microscale, the drawing force caused by crystallization shrinkage will have more greatly effect on the PP melt. Thus, it can be deduced that in comparison to neat PP melt, the drawing force generated in the spatial confinement will make the movement of PP chains more difficult. Then this effect must lead to the increasing of the activation energy of PP chain segments arranged into crystal naturally. As a result,

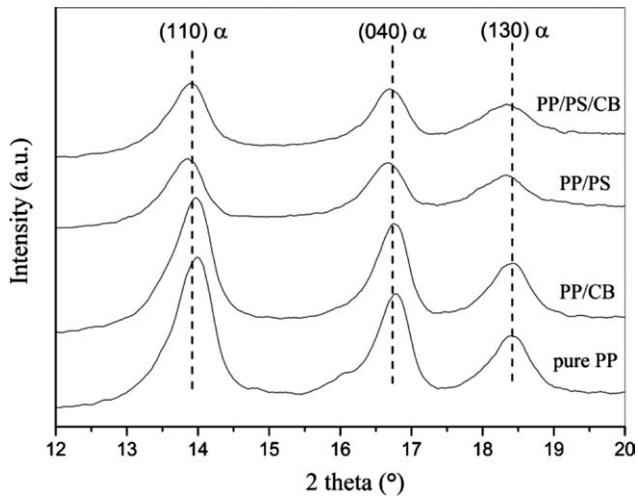

Figure 11 WAXD profiles of neat PP, PP/CB (100/1), PP/PS (55/45), and PP/PS/CB (55/45/1) isothermally crystallized at 122°C.

the crystal growth rate of PP in spatial confinement will be reduced obviously. These inferences are in good agreement with the results from Figure 3.

CONCLUSIONS

In this work, the effects of spatial confinement and selective distribution of CB Particles on the crystallization behavior of polypropylene were studied. The nonisothermal crystallization parameters analysis showed CB particles in the PP/CB composite and the continuous PS phase in the PP/PS blend could act as nucleating agents which obviously increased the crystallization temperature. For PP/PS/CB composite, the effect of heterogeneous nucleation of CB particles was weakened greatly because CB particles were distributed in PS phase. The results of the total crystallization activation energy (ΔE) and the nucleation parameter (K_g) implied that in comparison to neat PP, the diffusion activation energy of PP chain segments arranged into crystal was increased in PP/PS/CB with cocontinuous structure. It is believed that the crystallization occurred in the spatial confinement provides a good explanation for higher diffusion activation energy and lower spherulite radial growth rate for PP in composite.

References

1. Paul, D. R.; Barlow, J. W.; Keskkula, H. Encyclopedia of Polymer Science and Engineering; Wiley: New York, 1988.
2. Yin, B.; Zhao, Y.; Yu, R. Z.; An, H. N.; Yang, M. B. Polym Eng Sci 2007, 47, 14.
3. Kudva, R. A.; Keskkula, H.; Paul, D. R. Polymer 2000, 41, 239.
4. Vilcu, C.; Grigoras, C.; Vasile, C. Macromol Mater Eng 2007, 292, 445.
5. Bhattacharya, M.; Bhowmick, A. K. Polymer 2008, 49, 4808.
6. Zhang, Q. X.; Yu, Z. Z.; Xie, X. L.; Mai, Y. W. Polymer 2004, 45, 5985.
7. Papageorgiou, G. Z.; Achilias, D. S.; Bikiaris, D. N.; Karayannidis, G. P. Thermochim Acta 2005, 427, 117.
8. Chae, D. W.; Kim, B. C. Macromol Mater Eng 2005, 290, 1149.
9. Guan, Y.; Wang, S. H.; Zheng, A.; Xiao, H. N. J Appl Polym Sci 2003, 88, 872.
10. Arroyo, M.; Zitzumbo, R.; Avalos, F. Polymer 2000, 41, 6351.
11. Manchado, M. A. L.; Torre, L.; Kenny, J. M. J Appl Polym Sci 2001, 81, 1063.
12. Cho, K. W.; Li, F. K.; Choi, J. Polymer 1999, 40, 1719.
13. Yin, B.; Zhao, Y.; Pan, M. M.; Yang, M. B. Polym Adv Technol 2007, 18, 439.
14. Gan, D. J.; Lu, S. Q.; Song, C. S.; Wang, Z. J. Eur Polym J 2001, 37, 1359.
15. Zhang, Q. X.; Yu, Z. Z.; Yang, M. S.; Ma, J.; Mai, Y. W. J Polym Sci Polym Phys 2003, 41, 2861.
16. Ning, N. Y.; Luo, F.; Wang, K.; Zhang, Q.; Chen, F.; Du, R. N.; An, C. Y.; Pan, B. F.; Fu, Q. J Phys Chem B 2008, 112, 14140.
17. Saujanya, C.; Tangirala, R.; Radhakrishnan, S. Macromol Mater Eng 2002, 287, 272.
18. Li, T. Q.; Zhang, M. Q.; Zhang, K.; Zeng, H. M. Polymer 2000, 41, 161.
19. Deng, H.; Skipa, T.; Zhang, R.; Lellinger, D.; Bilotti, E.; Alig, I.; Peijs, T. Polymer 2009, 50, 3747.
20. Haggenmueller, R.; Fischer, J. E.; Winey, K. I. Macromolecules 2006, 39, 2964.
21. Paul, D. R.; Barlow, J. W.; Keskkula, H. Encyclopedia of Polymer Science and Engineering; Wiley: New York, 1988.
22. Persson, A. L.; Bertilsson, H. Polymer 1998, 39, 4183.
23. Dai, K.; Xu, X. B.; Li, Z. M. Polymer 2007, 48, 849.
24. Feng, J. Y.; Chan, C. M.; Li, J. X. Polym Eng Sci 2003, 43, 1058.
25. Yin, C. L.; Liu, Z. Y.; Yang, W.; Yang, M. B.; Feng, J. M. Colloid Polym Sci 2009, 287, 615.
26. Al-Saleh, M. H.; Sundararaj, U. Eur Polym J 2008, 44, 1931.
27. Wu, S. Polymer Interface and Adhesion; Marcel Dekker: New York, 1982.
28. Yang, H.; Zhang, X. Q.; Qu, C.; Li, B.; Zhang, L. J.; Zhang, Q.; Fu, Q. Polymer 2007, 48, 860.
29. Liu, S. Y.; Yu, Y. N.; Cui, Y.; Zhang, H. F.; Mo, Z. S. J Appl Polym Sci 1998, 70, 2371.
30. Avrami, M. J Chem Phys 1940, 8, 212.
31. Avrami, M. J Chem Phys 1939, 7, 1103.
32. Prat, C. F.; Hobbs, S. Y. Polymer 1976, 17, 12.
33. Hoffman, J. D.; Miller, R. L. Polymer 1997, 38, 3151.
34. Clark, E. J.; Hoffman, J. D. Macromolecules 1984, 17, 878.
35. Patel, R. M.; Spruiell, J. E. Polym Eng Sci 1991, 31, 730.
36. Avrami, M. J Chem Phys 1941, 9, 177.